doi:10.1016/j.neuroimage.2016.04.004

Automatic cortical surface reconstruction of high-resolution T_1 echo planar imaging data

Ville Renvall, Thomas Witzel, Lawrence L. Wald, and Jonathan R. Polimeni

Supplementary methods

T_1w image synthesis

We began by computing a T_1w magnitude-valued image from the fitted T_1 map using the Bloch equation model applied to a simplified MP-RAGE pulse sequence design; this assumes a single constant S_0 value across all voxels, removing the influence of ρ and T_2^* contrast. As in standard MP-RAGE, multiple lines of *k*-space are encoded after each inversion pulse during inversion recovery—all partitions in the inner phase-encoding loop (along k_z) are acquired during each inversion recovery, and the data acquired during each inversion recovery correspond to one step in the outer phase encoding loop (along k_y), thus the number of inversion pulses during the data acquisition is equal to the number of outer phase encoding steps. A left–right partition encoding direction was chosen, and in the simulation each partition was acquired at a distinct time after the inversion pulses and so was assigned a distinct effective *TI* where the time increment was equal to the MP-RAGE echo spacing. Therefore each k_z plane was assigned a different transfer function mapping the tissue parameters to signal levels based on the pulse sequence timing. The synthetic T_1w images were derived using the protocol parameter values *TR* = 4.5 s, *TI* = 2.2 s at the center of *k*-space (i.e. nominal *TI*), $\alpha = 7°$, nominal echo spacing (esp) = 6 ms, with signals computed at distinct *TI*s for groups of 8 k_z planes to emulate acceleration (Tisdall et al., 2013; van der Kouwe et al., 2014) or segmentation (Falkovskiy et al., 2013) of the inner phase encoding loop that would be measured with an acceleration factor of 8—this effectively decreases the total encoding time during each inversion recovery, which results in less weighting of *k*-space data by the T_1 recovery and therefore reduces image blurring (van der Kouwe et al., 2014).

These raw synthetic images were processed by *FreeSurfer* except in locations where outlier T_1 and S_0 values caused artifacts in the synthetic images. To improve consistency across subjects the raw synthetic images were lightly reweighted using scaled versions of the parameter maps obtained through fitting, especially to suppress fitting outliers, based on the observation that locations of extreme values in the T_1 and S_0 parameter maps tended to produce outlier values in the synthetic T_1w EPI images. Thus, after synthesizing the initial T_1w image, additional steps were taken to suppress these outlier values and thereby allow the EPI-based synthetic images to better resemble typical MP-RAGE image data. The steps included a reintroduction of T_2^*-weighting, and spatial homogenization of T_1 values or "T_1-deweighting" to reduce image variation within tissue classes and negate some imaging artifacts and parameter fitting outliers, followed by brain masking. Fig. S1 summarizes these preprocessing functions.

doi:10.1016/j.neuroimage.2016.04.004

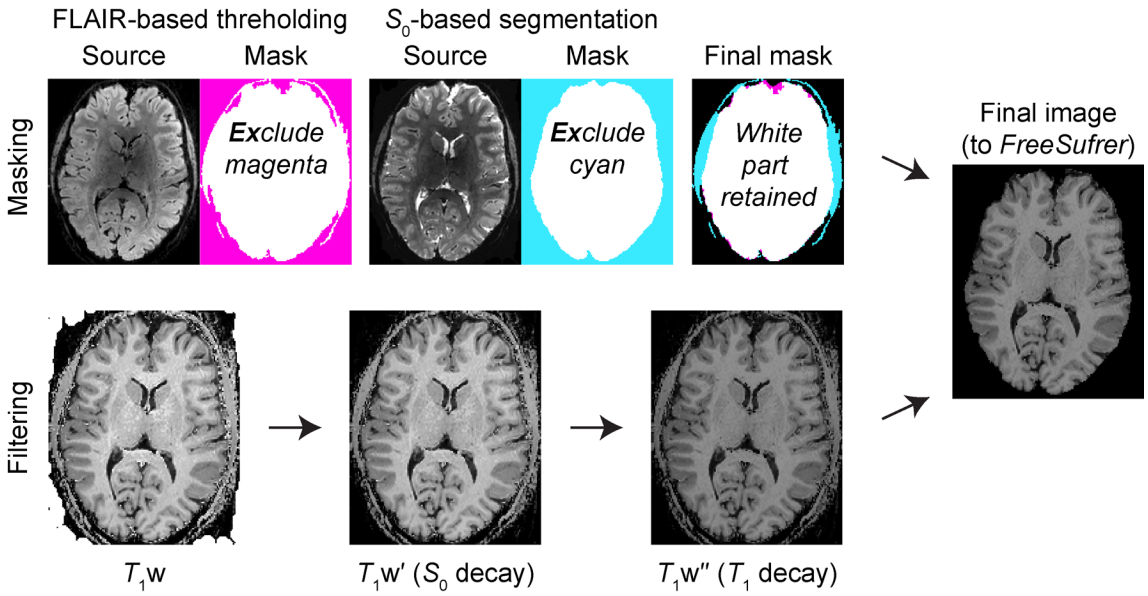

Fig. S1. Preprocessing steps following T_1-based contrast modeling. Brain extraction (top) is based on simple thresholding of the synthetic FLAIR-image, segmenting the S_0 image via SPM, and combining the exclusion masks. The intensity filtering of the T_1w MP-RAGE-resembling image (bottom) relies on exponential decay based on scaled S_0 and T_1 maps as described in the Supplementary methods text. First a multiplicative weighting is applied to the original T_1w image based on the scaled S_0 map to produce the image T_1w', then a second multiplicative weighting is applied based on the scaled T_1 map to produce the final image T_1w''.

To perform this filtering, a white matter (WM) mask was obtained from the S_0 map (using SPM12, http://www.fil.ion.ucl.ac.uk/spm (Ashburner and Friston, 1997)) such that every voxel with >95% probability of being WM was included in the mask. In order to reintroduce some T_2^* contrast into the synthetic images, we generated a rough approximation of a T_2^* map from the S_0 images which are predominantly T_2^* weighted. The T_2^* map was approximated by first globally scaling the S_0 map by a constant equal to the reported T_2^* value of WM at 7 T ($T_{2,WM}^*$ = 26.8 ms (Peters et al., 2007)) divided by the median image intensity of S_0 within the WM mask ($S_{0,WM}$), i.e., $S_0' = S_0 (T_{2,WM}^* / S_{0,WM})$. Using this approximate T_2^* map we generated a synthetic MP-RAGE image with T_2^* weighting given by $(T_1w') = (T_1w) \cdot \exp(-TE/S_0')$, where (T_1w) represents the intensities of the original nonscaled T_1w image. The TE was chosen so that the coefficient of variation (CV) of the image intensities of T_1w′ within the WM mask was minimized, with the constraint that $TE \geq 1$ ms. The addition of T_2^* weighting through this step helped reduce signal levels in regions outside of the brain and reduced high-level signals seen in blood vessels. The correction was in general subtle, as shown in Fig. S1, with TE mean $\pm$ standard deviation being 1.3 ± 0.5 ms. It should be noted that although here we assume that S_0' approximates T_2^*, S_0' contains also ρ. However, T_2^* and ρ are correlated, and the range of ρ in major tissue classes in the brain is relatively narrow, thus the impact of ρ on the filtering is small.

T_1 values are known to vary within cortical gray matter (GM), with systematic differences found in different cortical areas (Abbas et al., 2014), presumably due to e.g. varying myelin content. This heterogeneity across regions causes a spatially varying GM–WM contrast. Because we possess a quantitative T_1 map, these regional differences can be easily suppressed to improve the robustness of the tissue segmentation. To further promote signal homogeneity within tissue classes, we performed a similar procedure to the reintroduction of T_2^* contrast. In this T_1 homogenization step, we generated a spatial weighting term by first scaling the quantitative T_1 (similarly as for T_2^* above) such that the median of WM was again scaled to 26.8 ms, and the result was truncated so that the ceiling of the map was 20 ms; this scaled T_1 map is denoted as T_1'. Then, we calculated an exponential weighting term $\exp(-\tau/T_1')$, where, as with the generation of T_2w' described above, the value of τ was chosen to minimize the CV within WM with the constraint that $\tau \geq 1$ ms imposed to attenuate abnormally bright voxels. In Fig. S1, the result of this step is denoted as T_1w''. The T_1' decay suppresses outlier voxels in regions of low SNR and poor parameter fits. (In the context of segmentation, for *FreeSurfer* hypointense voxels within the WM are less problematic than hyperintense voxels.) Furthermore, because the T_1 map is the same data that is used in the T_1w synthesis, reusing it for T_1 homogenization flattened the within-tissue intensity distributions nonlinearly, being most effective at the T_1 values in hyperintense WM (where setting the maximum T_1'

value to 20 ms helped to only suppress these hyperintensities). Mean ± standard deviation of the τ for this step was 4.3 ± 3.3 ms.

Note that the two image weighting steps described above are not necessary to produce T_1-weighted EPI images approximating MP-RAGE contrast that are suitable for FreeSurfer, rather these steps can help to make the anatomical segmentation more robust. Both the reintroduction of T_2^* contrast and the homogenization of T_1 values clearly reduce the tissue contrast of the T_1w image (as seen in Fig. S1), but these weighting steps act to attenuate voxels with outlier T_2^* and T_1 values.

Brain mask

The *FreeSurfer* surface reconstruction is vulnerable to inaccuracies in the identified brain volume, called the `brainmask`, especially if the non-masked non-brain volume includes high voxel-intensities. Bright voxels can be confused for WM, and when this occurs the placement of both the WM–GM surface and the GM–CSF surface fails. Therefore, we generated a second synthetic volume for the sole purpose of producing an accurate brain mask. To do so, S_0 and T_1 maps were used to create images with CSF suppressed (similar to T_2^*-weighted fluid attenuated inversion recovery (FLAIR) images), using the expression $S(TI) = S_0 - 2S_0 \exp(-TI/T_1)$, which is the model for ideal inversion recovery sequence at the limit where $TR >> T_1$. Instead of using only one TI in the model, a range of TI values were computed and the minimum intensity for each voxel in the volume was selected from this set. In effect, this procedure generates a more reliable fluid attenuation than using only one parameter value, and it picks the intensities of WM and GM at the lowest TI, given a sufficiently long TI. The TI range used for the FLAIR syntheses was set to 2.6–6.0 s (with 0.1 s spacing); the long TI values ensured that not only signal from WM and GM would be positive-valued (i.e., past the zero-crossing of the inversion recovery), but also the CSF intensity was for the great majority of voxels positive yet still sufficiently dark. A fixed threshold of 1000 (arbitrary units; corresponding to about 50% of the GM intensity) was used for all datasets as it produced consistent results across subjects. The resulting binary image was segmented and the main brain volume was extracted automatically, after which the holes in this brain volume mask were filled through a floodfill algorithm.

Additionally, the S_0-based segmentations (obtained with SPM12, as described above) were used to create masks containing the WM, GM and CSF partitions, and these masks were combined with those of the FLAIR mask. These latter mask components were used to remove some connected non-brain tissue surviving the FLAIR mask. Finally, the combined masks were applied to the filtered T_1w EPI images. Examples of the FLAIR image, FLAIR-based mask, S_0 source image, the derived segmentation-based mask, and a final combined mask are presented in Fig. S1.

Quantification of resampling blur due to B_0 field map -based distortion correction

To compare our proposed strategy of generating surfaces directly from EPI data that are distortion-matched to the functional data with the conventional strategy of dewarping the EPI data to match with surfaces generated from MP-RAGE data, we applied standard geometric distortion correction techniques to the EPI data using conventional B_0 field maps. Because dewarping causes image resampling and therefore blurring, we quantified the resolution loss as follows: Time-series EPI BOLD data were dewarped using the 'epidewarp.fsl' utility in *FreeSurfer* (that is a wrapper around FSL Prelude (Jenkinson, 2003) and Fugue (Jenkinson, 2001; Jezzard and Balaban, 1995) programs) and a separately acquired B_0 field map. The resulting dewarping field produced by Fugue was then applied to image volumes of synthetic Gaussian white noise that were the same the size of the BOLD volumes. The standard deviation (σ) across the time dimension was computed at each voxel of the dewarped noise matrix. To compute the effective spatial smoothing induced by the dewarping process, the original untouched noise matrix was spatially smoothed using a range of kernel widths of 1-dimensional Gaussians (since voxel shifting and therefore resampling blur occurs only in the phase-encoding direction), then the temporal σ was computed for each smoothing kernel, and a lookup table was constructed between temporal σ and the full-width-at-half-maximum (FWHM) of the spatial smoothing kernel. Finally, the corresponding FWHM values were found for the voxels in the warped noise matrix based on the temporal σ.

doi:10.1016/j.neuroimage.2016.04.004

Supplementary results

To illustrate how the contrast varies across slices and slice permutations during the acquisition, four (out of 18) example frames of MI-EPI images are presented in Fig. S2, with finer details of one slice shown of every frame, reordered by *TI* value.

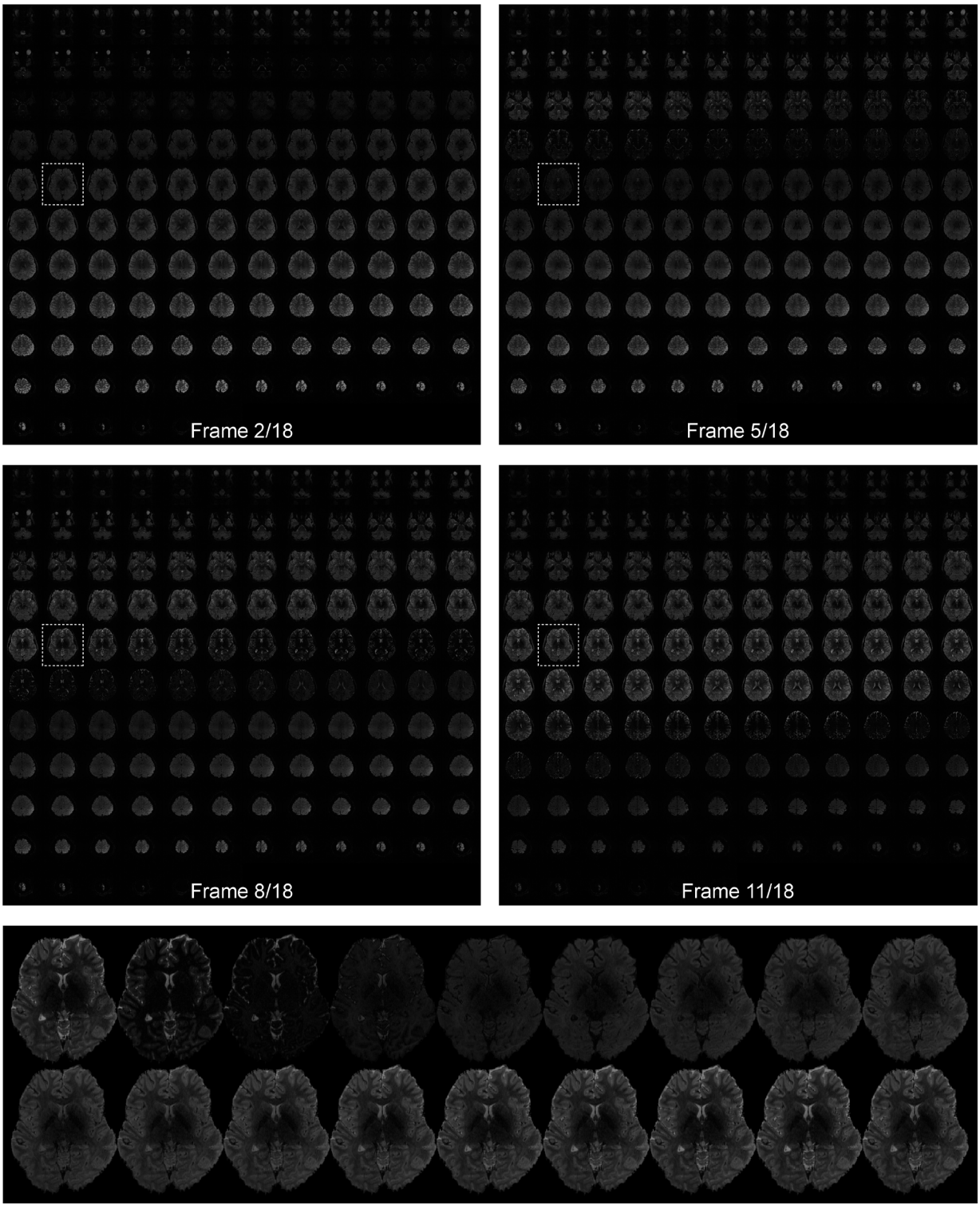

Fig. S2. Image frames from an MI-EPI acquisition. The image contrast varies across slices and frames (top) as the effective *TI* is modulated by the slice permutation, here with a shift factor N_{shift} = 7. The dotted square indicates the slice shown in more detail at the bottom, where the 18 different contrast images of that slice are shown in ascending *TI* order.

doi:10.1016/j.neuroimage.2016.04.004

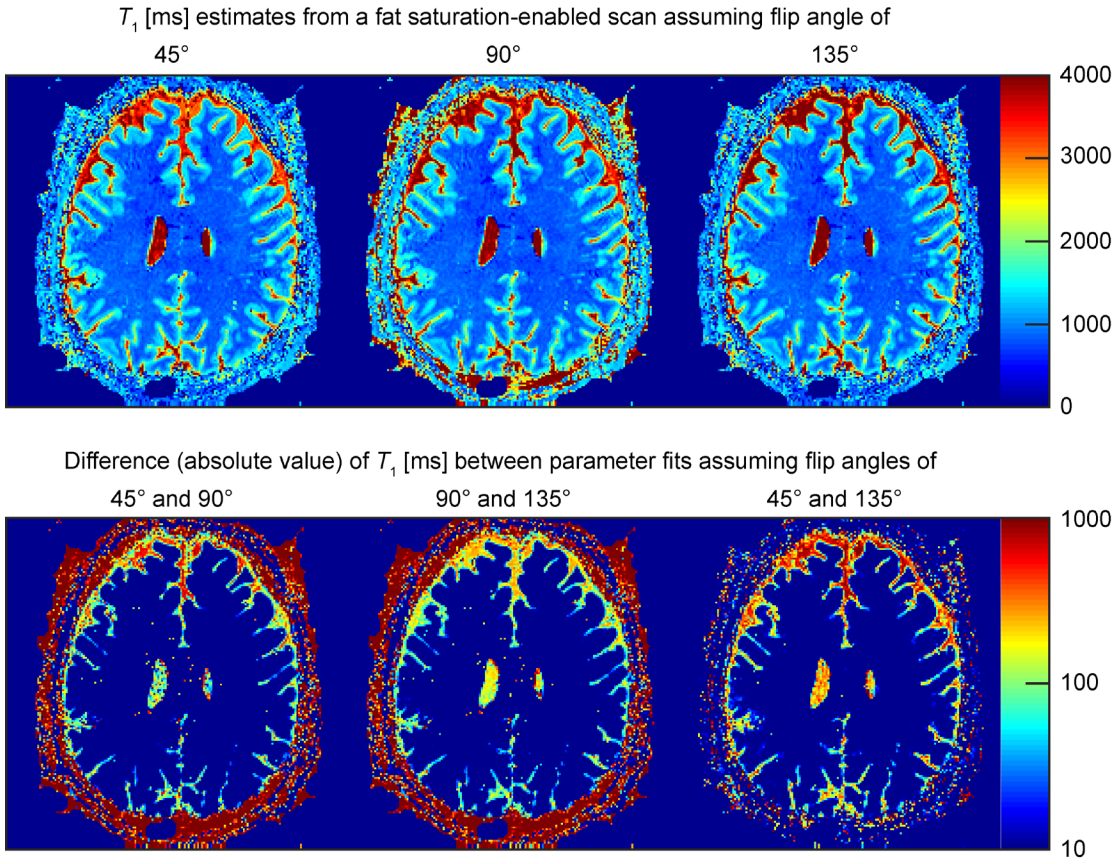

Fig. S3. Comparison of estimated T_1 values when the fitting routine is given a fixed flip angle of 45°, 90° or 135°. For short to medium T_1 values present in WM and GM, the differences in estimation are negligible. For CSF, with a long T_1, the variability of flip angle would cause a bias depending on the excitation angle. All other parameters in the simulation are set according to the acquisition protocol.

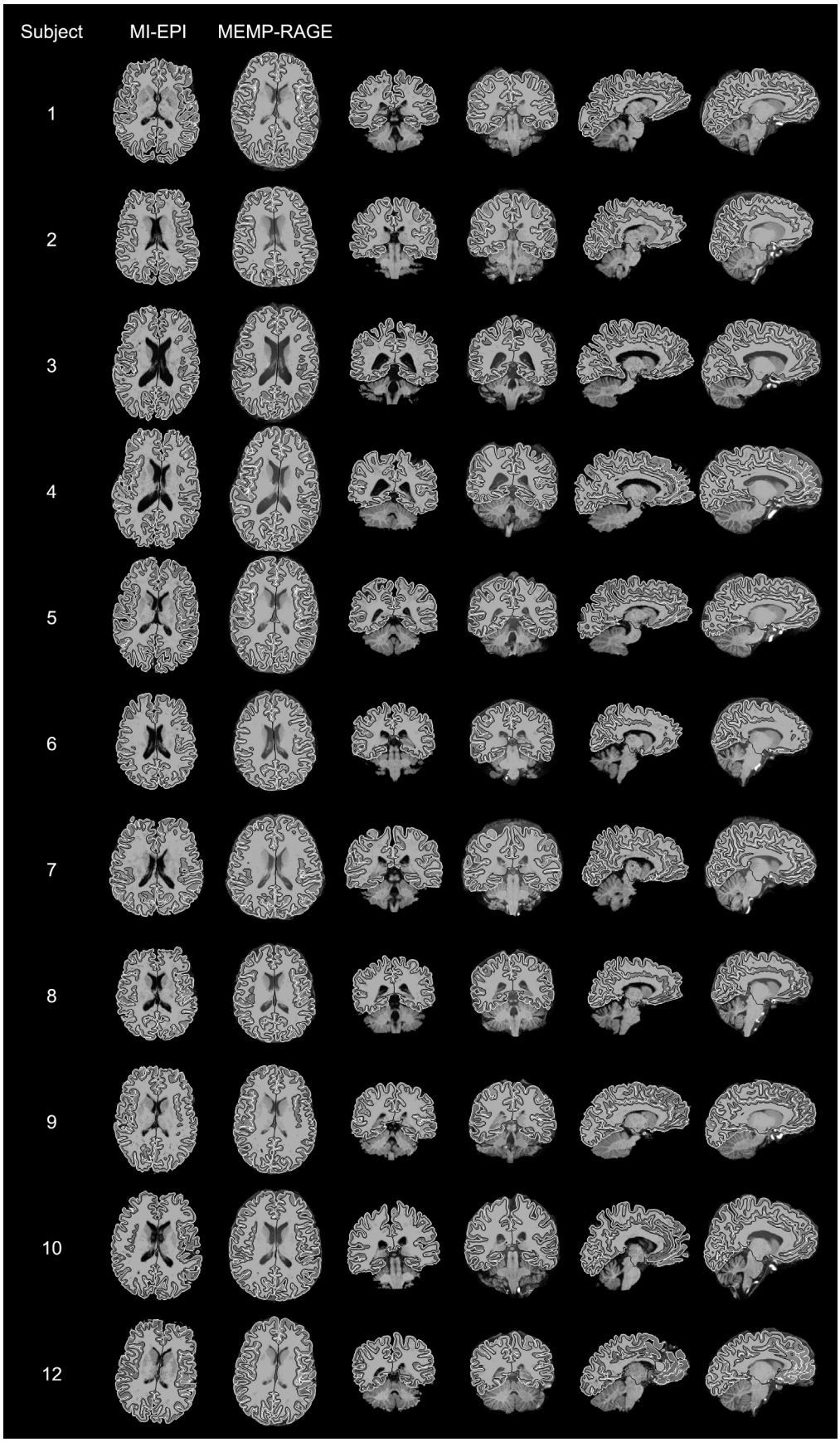

Fig. S4. Comparison of T_1w EPI and MEMP-RAGE images and surface reconstructions. Axial, coronal and left hemisphere sagittal slices are shown for every subject at approximately same locations for both image modalities. The images are in their own post-*FreeSurfer* image matrices instead of co-registered in order to show both image modalities neutrally. Black and white lines shown on the images represent the white and pial surfaces, respectively.

doi:10.1016/j.neuroimage.2016.04.004

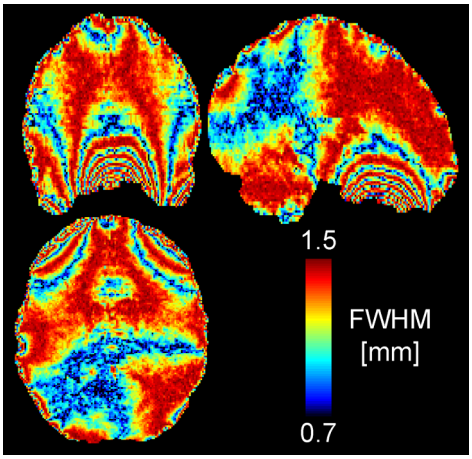

Fig S5. Blurring induced by B_0 field map -based geometric distortion correction. The variation of the blur reflects the susceptibility-induced field variation. At the maximum FWHM, the resampling blur corresponds to unweighted averaging of intensities of adjacent voxels.

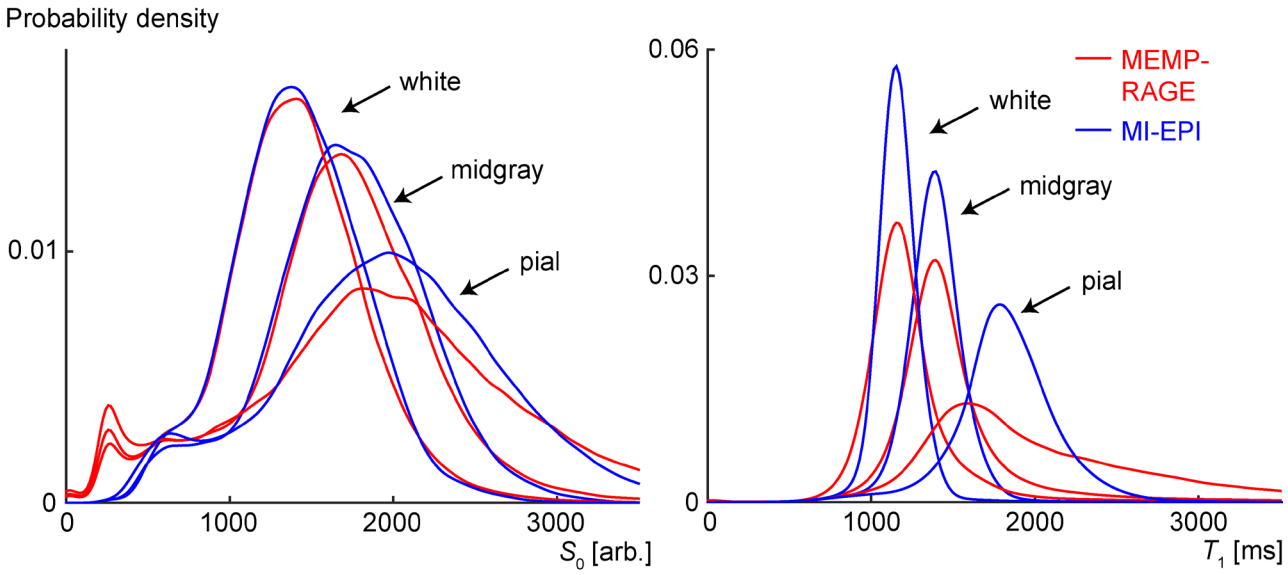

Fig. S6. Distribution of parameter values sampled by the cortical surface reconstructions. The S_0 (left) and T_1 (right) panels show the parameter value distributions from voxels intersecting the white, midgray, and pial surfaces for MEMP-RAGE (red) and MI-EPI (blue) reconstructions. Data is from *a single representative subject*.

doi:10.1016/j.neuroimage.2016.04.004

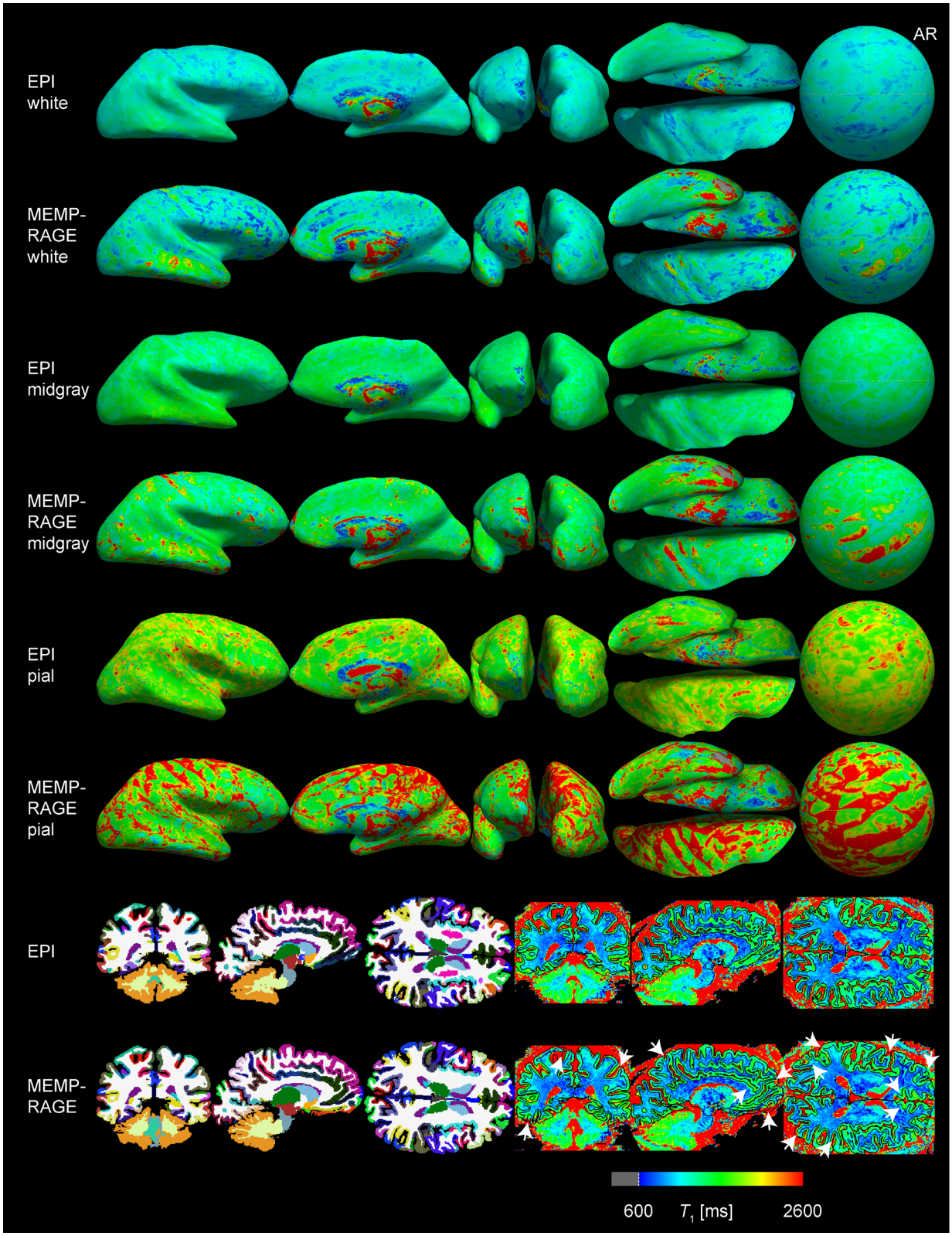

Fig. S7. Comparison of the sampling of T_1 by surfaces based on EPI and MEMP-RAGE anatomical reference images in a single subject. The T_1 sampled by the white, midgray, and pial surfaces are shown for the inflated right hemisphere of one subject from different viewing directions, from left to right: lateral, medial, anterior, posterior, inferior (top), and superior (bottom). The spherical half-hemisphere projection is viewed from the superior direction, with anterior right (AR) location indicated. The bottom–right shows, on the same color scale than the surface sampling illustrations, the placement of the white and pial surfaces overlaid on the coronal, sagittal and axial brain sections of the T_1 map; white arrows indicate places where the misalignment of the MEMP-RAGE surfaces with respect to the T_1 (and S_0) map is particularly clear. Additionally, to demonstrate the success and similarity of the automatically processed brain segmentations and cortical parcellations between the EPI and MEMP-RAGE reconstructions, regional *FreeSurfer* labels are shown by different colors in the bottom–left.

doi:10.1016/j.neuroimage.2016.04.004

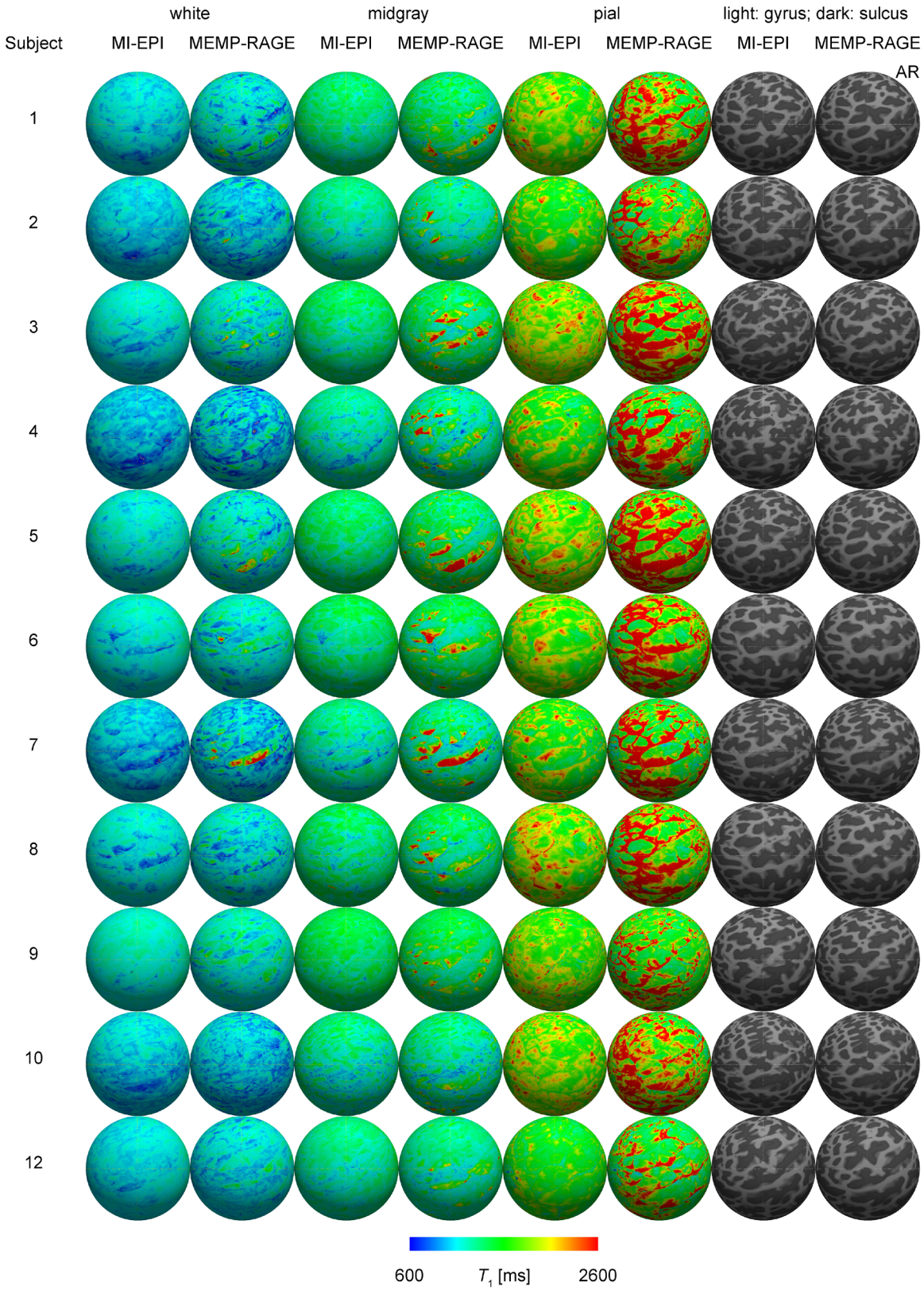

Fig. S8. Comparison of T_1 sampling by EPI and MEMP-RAGE surfaces in eleven subjects scanned at 7 T. The superior views of the inflated right half-hemisphere are shown for all subjects from which both MI-EPI and MEMP-RAGE data were available. The rightmost two columns show the cortical folding patterns where light gray represents gyri and dark gray sulci. The colorbar indicates the T_1 values sampled by the surfaces. The data were acquired using fat saturation, so that the T_1 estimates presented here are expected to be lower than the actual values, e.g. T_1 is expected to be below 1900 ms for GM.

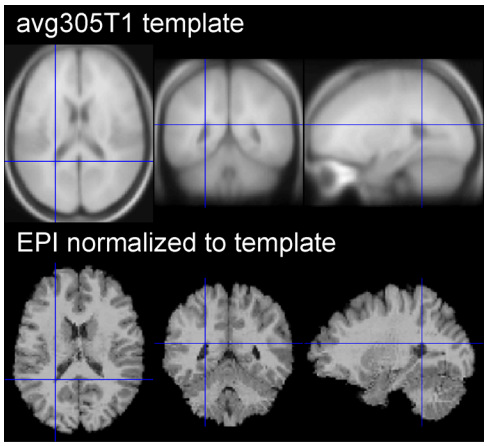

Fig. S9. T_1w EPI normalized to MNI template. The T_1w EPI volume (bottom) was normalized to the MNI space (T_1w template image shown on the top) using SPM12.

References

Abbas, Z., Gras, V., Möllenhoff, K., Keil, F., Oros-Peusquens, A.-M., Shah, N.J., 2014. Analysis of proton-density bias corrections based on T1 measurement for robust quantification of water content in the brain at 3 Tesla. Magn. Reson. Med. 72, 1735–1745. doi:10.1002/mrm.25086

Ashburner, J., Friston, K., 1997. Multimodal image coregistration and partitioning--a unified framework. Neuroimage 6, 209–17. doi:10.1006/nimg.1997.0290

Falkovskiy, P., Kober, T., Reyes, D., Steinert, K., Seeger, M., Bernstein, M., Krueger, G., 2013. Segmented multi-echo MPRAGE acquisition for accelerated T1-weighted brain imaging, in: Proc. Intl. Soc. Mag. Reson. Med. Salt Lake City, p. 3703.

Jenkinson, M., 2001. Improved unwarping of EPI images using regularised B0 maps. Neuroimage 13, 165. doi:10.1016/S1053-8119(01)91508-3

Jenkinson, M., 2003. Fast, automated, N-dimensional phase-unwrapping algorithm. Magn. Reson. Med. 49, 193–7. doi:10.1002/mrm.10354

Jezzard, P., Balaban, R.S., 1995. Correction for geometric distortion in echo planar images from B0 field variations. Magn. Reson. Med. 34, 65–73. doi:10.1002/mrm.1910340111

Peters, A.M., Brookes, M.J., Hoogenraad, F.G., Gowland, P.A., Francis, S.T., Morris, P.G., Bowtell, R., 2007. T2* measurements in human brain at 1.5, 3 and 7 T. Magn. Reson. Imaging 25, 748–753. doi:10.1016/j.mri.2007.02.014

Tisdall, M.D., Polimeni, J.R., Augustinack, J., van der Kouwe, A.J.W., 2013. 350 µm isotropic, high-contrast, low-blur, low-distortion MPRAGE morphometry acquisition at 3T, in: 19th Annual Meeting of the Organization for Human Brain Mapping. Seattle.

van der Kouwe, A.J.W., Tisdall, M.D., Bhat, H., Fischl, B., Polimeni, J.R., 2014. Multiple echo and inversion time MPRAGE with inner loop GRAPPA acceleration and prospective motion correction for minimally distorted multispectral brain morphometry, in: Proc. Intl. Soc. Mag. Reson. Med. Milan, p. 120.